Xiang Ma
College of Electromechanical Engineering,
Qingdao University of Science and Technology,
99, Songling Road,
Qingdao City 266061, China
e-mail: maxiang7632@126.com

Wei Li[1]
College of Electromechanical Engineering,
Qingdao University of Science and Technology,
99, Songling Road,
Qingdao City 310027, China;
Department of Energy Engineering,
Zhejiang University,
38 Zheda Road,
Hangzhou 310027, China
e-mail: weili96@zju.edu.cn

Chuan-cai Zhang
College of Electromechanical Engineering,
Qingdao University of Science and Technology,
99, Songling Road,
Qingdao City 266061, China
e-mail: zhangchuancai2633@qq.com

Zhi-chuan Sun
Department of Energy Engineering,
Zhejiang University,
38 Zheda Road,
Hangzhou 310027, China
e-mail: sunzhichuan@zju.edu.cn

David J. Kukulka
Department of Mechanical Engineering
Technology,
State University of New York College at Buffalo,
1300 Elmwood Avenue,
Buffalo, NY 14222
e-mail: david_kukulka@hotmail.com

Yan He
College of Electromechanical Engineering,
Qingdao University of Science and Technology,
99, Songling Road,
Qingdao City 266061, China
e-mail: heyan_sd@163.com

Nae-Hyun Kim
Department of Mechanical Engineering,
Incheon National University,
12-1, Songdo-Dong, Yeonsu-Gu,
Incheon 22012, South Korea
e-mail: knh0001@inu.ac.kr

Zhixiao Zhang
School of Mechanical Engineering,
Hangzhou Dianzi University,
Hangzhou 310018, China
e-mail: zhixiaozh@hdu.edu.cn

Condensation and Evaporation Heat Transfer Characteristics of Low Mass Fluxes in Horizontal Smooth Tube and Three-Dimensional Enhanced Tubes

An experimental investigation of condensation and evaporation heat transfer characteristics was performed in 15.88-mm-OD and 12.7-mm-OD smooth and three-dimensional enhanced tubes (1EHT, 3EHT) using R134A and R410A as the working fluid. The enhanced surface of the 1EHT tube is made up of dimples and a series of petal arrays; while the 3EHT tube is made up of rectangular cavities. Evaluations are performed at a saturation temperature of 45 °C, over the quality range of 0.8–0.2 for condensation; while for evaporation the saturation temperature was 6 °C and the quality ranged from 0.2 to 0.8. For condensation, the enhancement ratio (enhanced tube/smooth tube) of the heat transfer coefficients was 1.42–1.95 for the mass flux ranging from 80 to 200 kg/m²s; while for evaporation, the heat transfer enhancement ratio is 1.05–1.42 for values of mass flux that range from 50 to 180 kg/m²s. Furthermore, the 1EHT tube provides the best condensation and evaporation heat transfer performance, for both working fluids at the mass flux considered. This performance is due to the dimples in the enhanced surface that produce interface turbulence; additionally, the increased surface roughness causes additional disturbances and secondary flows near the boundary, producing higher heat fluxes. The main objective of this study was to evaluate the heat transfer enhancement of two enhanced tubes when using R134A and R410A as a function of mass flux, saturation temperature, and tube diameter. As a result of this study, it was determined that the heat transfer coefficient decreases with an increase in saturation temperature and tube diameter. [DOI: 10.1115/1.4044172]

Keywords: condensation, evaporation, heat transfer coefficient, enhanced tubes, heat exchangers

Introduction

Two-phase flow studies have attached the attention of a variety of researchers in recent years. Condensers and evaporators are commonly used in various industrial systems (the refrigerators, air conditioners, heat pump, etc.). In order to improve the efficiency of

these heat exchangers, the field of the enhanced heat transfer technology has become an important consideration; many works have evaluated methods to generate higher heat transfer coefficients. Enhanced heat transfer tubes have become an important consideration in the desire to increase performance; these tubes directly affect the efficiency and energy consumption of the heat exchanger. Over time, various types of enhanced tubes have been developed and are widely used in industrial production to improve the heat transfer coefficients.

There are many types of enhanced tubes, they include micro-fin, herringbone, corrugated, flattened, and dimpled tubes. Several previous studies [1–10] on the condensation and evaporation heat transfer characteristics of these tubes have been performed.

Miyara et al. [11] studied the condensation performance of horizontal micro-fin and herringbone tubes. Kim [12] investigated the effect of various parameters on the tube-side condensation of micro-fin tubes using R410A. Sarmadian et al. [13] performed condensation experiments of R600a in horizontal, smooth, and helically dimpled tubes with a mass flux that varied from 114 to 368 kg/m^{2}s. Aroonrat and Wongwises [14] studied the condensation heat transfer and pressure drop characteristics of R134a flowing inside horizontal smooth and dimpled tubes (8.1 mm in diameter and 1500 mm in length) at saturated temperatures of 30 °C, 40 °C, and 50 °C. From the results, it appears that the average heat transfer coefficient and the frictional pressure drop tend to increase with an increasing average vapor quality and mass flux. The Nusselt number of the dimpled tubes are 1.3–1.4 times larger than those found in a smooth tube for similar conditions and the two-phase friction factor is 2.8–4.1 times larger. In the studies [15,16], condensation heat transfer and pressure drop results of the dimpled tubes with different helical, dimpled pitches, and depths are also found. Li et al. [17] showed an experimental investigation of the shell-side flow condensation inside a smooth tube and 2EHT enhanced tubes. They analyzed the effect of the saturated temperature, mass flux, and vapor quality on the heat transfer coefficients; they also present a new heat transfer model (based on the Nusselt's theory) for outside condensation.

A number of studies (Dalkilic et al. [18], Lu et al. [19], Jiangzhi et al. [20], Guo et al. [21]) evaluated the evaporation heat transfer coefficient of micro-fin tubes for a variety of parameters. Guo et al. [21] performed an experimental investigation on the condensation and evaporation heat transfer characteristics for various refrigerants (R22/R32/R410A) inside smooth, herringbone, and enhanced surface tubes. Mass flux ranged from 55 to 181 kg/(m^{2}s) and heat flux ranged from 9.8 to 36 kW/m^2, with the vapor quality ranging from 0.1 to 0.9. The results showed that the condensation heat transfer coefficient of the 1EHT is about 1.3–1.95 times larger than that of a smooth tube; however, the herringbone tube produced the highest condensation heat transfer enhancement. For evaporation, the 1EHT tube produced the highest evaporation heat transfer performance when using R22/R32/R410A. The authors found the Cavallini et al. correlation [22] to predict condensation results for a smooth tube and the modified Wojtan et al. correlation [23] to predict evaporation results. Li et al. [24] tested the heat transfer coefficients and friction pressure drop during the condensation and evaporation of R410A inside a horizontal smooth tube and 2EHT tubes. They showed that the evaporation heat transfer coefficient of 2EHT tubes is 11–44% larger than that of the smooth tube, and 10–16% larger for condensation. Wang et al. [25] obtained the condensation heat transfer and pressure drop characteristics of R134A inside a plain tube and four enhanced tubes with different pin fins structures, for saturation pressures of 13.4 bars and 11.6 bars. They conducted the experiments for a mass flux range of 50–150 kg/m^{2}s. They concluded that the heat transfer coefficient of the four enhanced tubes is about 1.5–2.5 times that of the smooth tube.

The purpose of this investigation is to study the condensation and evaporation heat transfer characteristics at a low mass flux for 15.88-mm-OD and 12.7-mm-OD enhanced tubes (1EHT/3EHT) and compare the results with a smooth tube using R410A and R134A. During the experiment, the average heat transfer coefficient is determined and the effect of saturation temperature and tube diameter on the condensation and evaporation heat transfer coefficients was also discussed. Finally, experimental data were compared with previously reported empirical models.

Experimental Apparatus and Procedure

Schematic diagram of the experimental system used for this investigation is given in Fig. 1(a); it consisted of a preheat section, a test section, and a subcooling section. The experimental apparatus has been previously used and discussed in Refs. [2,3]. As can be seen in Fig. 1, the preheat section controls the inlet vapor quality that enters into the test section, it is accomplished by changing the water temperature and mass velocity. The test section is shown in Fig. 1(b); it consists of a straight, horizontal, counterflow, tube-in-tube heat exchanger (heating length of two meters). The refrigerant flows into the tube side, water flows through the shell side to heat/cool the refrigerant. The entire test section was insulated (in order to minimize the heat loss) using polyurethane rigid foam and rubber foam.

During the experiment, the refrigerant and water temperature were measured by a Platinum 100 RTD at the inlet and outlet of the preheat and test section, respectively. All the thermocouples were calibrated with an uncertainty of ±0.1 °C. The pressure transducers (with an accuracy of 0.075% of the full scale) at the inlet and outlet of the test section were installed to measure the refrigerant pressure; a differential pressure transducer was located between the inlet and outlet of the test section in order to obtain the total pressure drop. A Coriolis mass flow meter (with an accuracy of 0.2% of full scale) was used to measure the mass flux between 50 and 200 kg/m^{2}s in this refrigerant loop.

Figure 2 shows the three-dimensional view and surface structures of the enhanced tubes (1EHT/3EHT). Tested tubes include (a) a stainless steel smooth tube with outer diameter of 15.88-mm-OD and 12.7-mm-OD; (b) 1EHT stainless steel tube, as shown in Fig. 2(a), the surface structure of the 1EHT tube is composed of dimpled protrusions with secondary petal arrays. There are five rows of main rounded dimples, in which the depth of the dimple is 2.36 mm and the diameter of the dimple is 3.00 mm; and (c) 3EHT stainless steel tube, as shown in Fig. 2(b), unlike a 1EHT tube, the enhancement structure of the 3EHT tube is a series of rectangular cavities and grooves. The length, width, and depth of rectangular cavities are 7.20 mm, 3.20 mm, and 1.00 mm, respectively. Obviously, these surface enhancement structures can increase the heat transfer area and provide more heat flux. The inner heat transfer area of the 1EHT tube is approximately 1.20 times than that of the smooth tube; for the 3EHT tube, it has a heat transfer area ratio (A_e/A_s) that is 1.25. Three tested tubes have the same outer diameter (d_o) of 15.88 mm.

Condensation tests using R134A and R410A were conducted at saturation temperatures of 35 °C, 40 °C, and 45 °C, with a mass flux ranging from 80 to 200 kg/(m^{2}s), heat flux range from 11 to 29 kW/m^2, with an inlet vapor quality of 0.8, and an outlet vapor quality of 0.2. Evaporation heat transfer tests using R134A and R410A are investigated at a saturation temperature of 6 °C and 10 °C; with a mass flux ranging from 50 to 180 kg/(m^{2}s), heat flux in the range from 9 to 35 kW/m^2, and a vapor quality that varies from 0.2 to 0.8. The summary of the operating conditions is given in Table 1. During the experiment, the inlet and outlet vapor quality values remained constant; mass flux and heat flux varied. Experimental data were collected every ten continuous data points (time interval of every data is 20 s) when the deviations of temperature, pressure, and vapor quality were below 0.1 °C, 3 kPa, and 0.05, respectively. All thermodynamic properties of refrigerant (R134 and R410A) and water were acquired from NIST REFPROP 9.0 database [26] shown in Table 2.
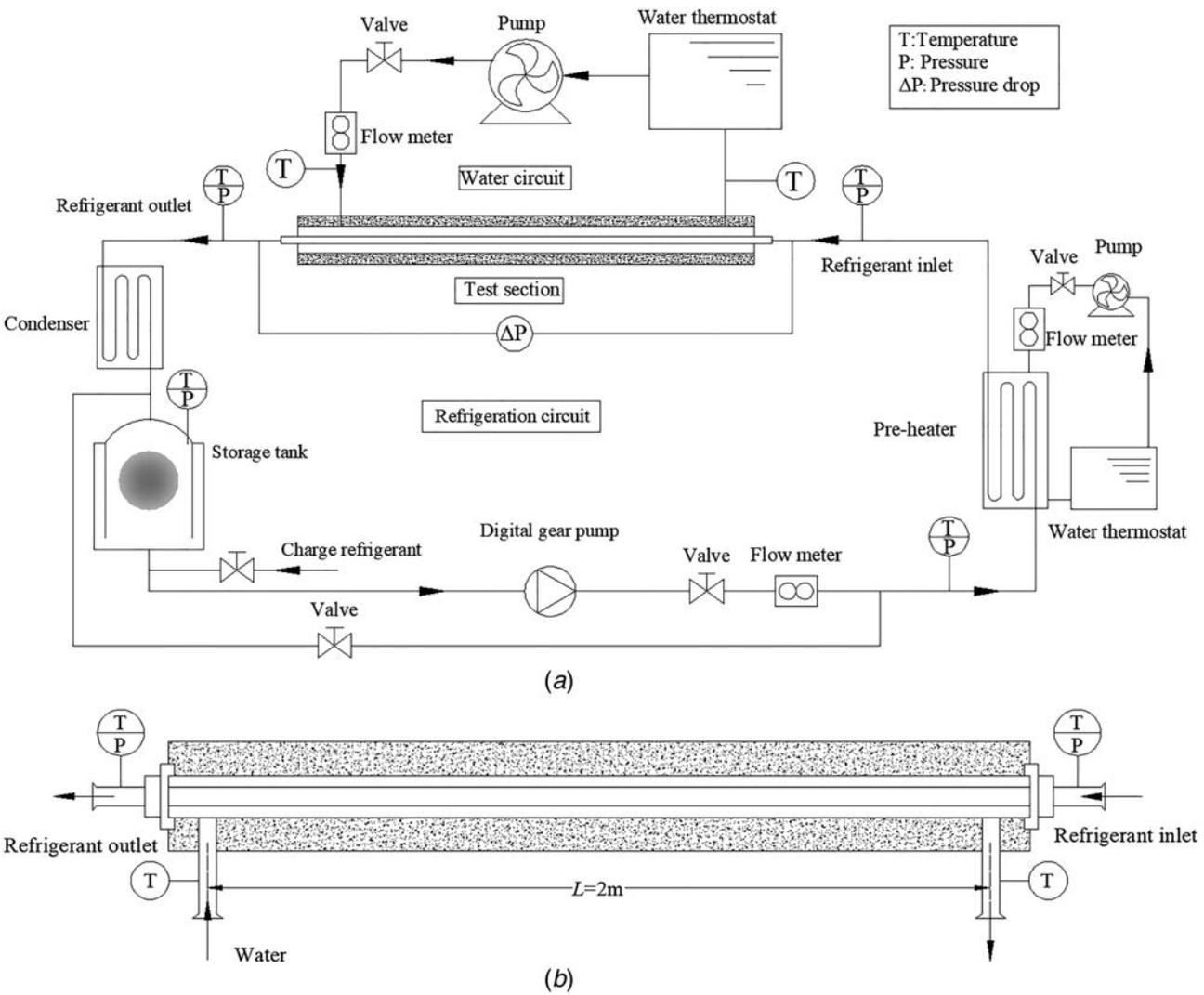
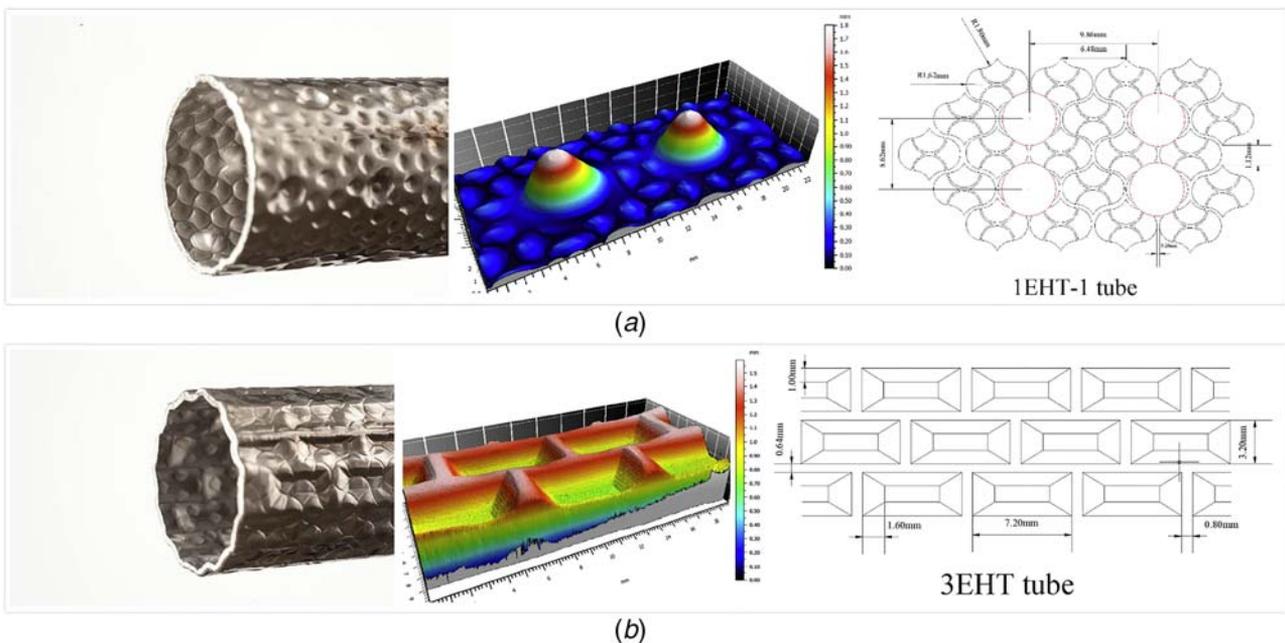**Fig. 1   Schematic of the experimental system**

Fig. 2   Views of the inner surface and outer surface of the (*a*) 1EHT tube and (*b*) 3EHT tube

Table 1 Operating conditions

Controlled variable	Condensation	Evaporation
Refrigeration	R134A/R410A	R134A/R410A
Saturation temperature	35 °C/40 °C/45 °C	6 °C/10 °C
Mass flux	80–200 kg/m^{2}s	50–180 kg/m^{2}s
Heat flux	14–25 kW/m^2	9–35 kW/m^2
Vapor quality	0.8–0.2	0.2–0.8

Data Reduction. The total heat transfer flux is determined by the heat balance of the water flowing through the heat exchanger in the test section

$$Q_{w,exp} = c_{p,w,exp} m_{w,exp}(T_{w,exp,out} - T_{w,exp,in}) \qquad (1)$$

where $m_{w,exp}$, is the water mass flux through the whole test section; $T_{w,exp,out}$ and $T_{w,exp,out}$ are the annulus inlet and outlet water temperature at the test section, respectively.

The refrigerant heat flux of the test section can be determined as

$$Q_{ref,exp} = m_{ref,exp}(H_{ref,exp,in} - H_{ref,exp,out}) \qquad (2)$$

where $m_{ref,exp}$ is the refrigerant mass flux of the test section and $(H_{r,exp,in} - H_{r,exp,out})$ is the refrigerant specific enthalpies difference between the inlet and outlet of the test section.

Hence, the heat loss between the water and refrigerant sides was calculated by the energy balance equation

$$\gamma = \frac{|Q_{w,exp} - Q_{ref,exp}|}{Q_{w,exp}} \times 100\% \qquad (3)$$

The inlet vapor quality (x_{in}) can be calculated as follows:

$$x_{in} = \frac{Q_{pre} - c_{p,ref,pre} m_{ref}(T_{sat} - T_{ref,pre,in})}{m_{ref} h_{lv}} \qquad (4)$$

where T_{sat} and h_{lv} are refrigerant saturated temperature and the latent heat of vaporization of refrigerant taken at the saturated temperature, respectively.

The outlet quality of the test section (x_{out}) is calculated by

$$x_{out} = x_{in} \pm \frac{Q_{w,exp}}{m_{ref} h_{lv}} \qquad (5)$$

The log-mean temperature difference ($LMTD$) is determined by

$$LMTD = \frac{(T_{w,exp,in} - T_{ref,exp,out}) - (T_{w,exp,out} - T_{ref,exp,in})}{\ln\left[(T_{w,exp,in} - T_{ref,exp,out})/(T_{w,exp,out} - T_{ref,exp,in})\right]} \qquad (6)$$

Assuming there is no fouling resistance, the tube-side refrigerant heat transfer coefficient for condensation or evaporation can be expressed by the following resistance model

$$h_i = \frac{1}{A_i\left[\dfrac{LMTD}{Q_{ref,exp}} - \dfrac{1}{h_o A_o} - \dfrac{d_o \ln(d_o/d_i)}{2k A_o}\right]} \qquad (7)$$

In Eq. (7), A_i and A_o are the nominal internal and external heat transfer area based on d_i and d_o of the test tubes, respectively; k is the thermal conductivity of tube material (stainless steel $k = 17$ W/m K).

Gnielinski correlation [27] can predict the shell-side heat transfer coefficients accurately for a smooth tube and is only valid for $0.5 < Pr < 2000$ and $3000 < Re < 5 \times 10^6$. Hence, Gnielinski equation was used to calculate the water-side heat transfer coefficient h_o

$$h_o = \frac{(f/2)(\text{Re}_w - 1000)\text{Pr}}{1 + 12.7(f/2)^{0.5}(\text{Pr}^{2/3} - 1)}\left(\frac{\mu_{bulk}}{\mu_{wall}}\right)^{0.14}\frac{k_w}{d_h} \qquad (8)$$

The property ratio $(\mu_{bulk}/\mu_{wall})^{0.14}$ is a temperature difference factor reflecting the effect of the temperature distribution on the fluid properties. Additionally, k_w and d_h are the thermal conductivity of water and the shell-side hydraulic diameter ($d_h = D - d_o$).

The Fanning friction ratio is calculated by the Petukhov correlation [28] for $3000 < \text{Re} < 10^6$

$$f = (1.58 \ln \text{Re}_w - 3.28)^{-2} \qquad (9)$$

However, the Gnielinski correlation [27] cannot be directly used to calculate the annulus side heat transfer coefficients due to the existence of the dimples and rectangular cavities on the outer surface of the 1EHT tube and 3EHT tube. Therefore, the Wilson plot method needs to be used in order to obtain the enhancement ratio (C) of the two enhanced tubes.

Figure 3 shows the thermal resistance model for a circular tube. The corrected total resistance of the test section can be expressed by the following equation

$$\frac{1}{UA_o} = \frac{1}{C \cdot h_o A_o} + \frac{1}{h_i A_i} + \frac{d_o \ln(d_o/d_i)}{2k A_o} \qquad (10)$$

where $1/(UA_o)$ is the total thermal resistance, $1/(h_i A_i)$ is the inner tube thermal resistance, $d_o \ln(d_o/d_i)/(2k A_o)$ is the tube wall thermal resistance.

The theoretical basis of the Wilson plot method is given in Fig. 4. As the tube-side refrigerant mass velocity (V_{ref}) increases, the total thermal resistance $1/(UA_o)$ is considered as a function of $V^{-0.8}$. Hence, when the refrigerant mass flux is infinite, the tube-side thermal resistance, $1/(h_i A_i)$, tends to zero and the total thermal resistance, $1/(UA_o)$, can be approximately equal to the shell-side thermal resistance, $1/(h_o A_o)$ and the tube wall thermal resistance, $d_o \ln(d_o/d_i)/(2k A_o)$. In addition, in order to ensure both tube-side and shell-side turbulence, evaluations were conducted by changing the water mass flux and the refrigerant mass flux while keeping the tube wall thermal resistance fixed.

Table 2 Thermophysical properties of R134A and R410A

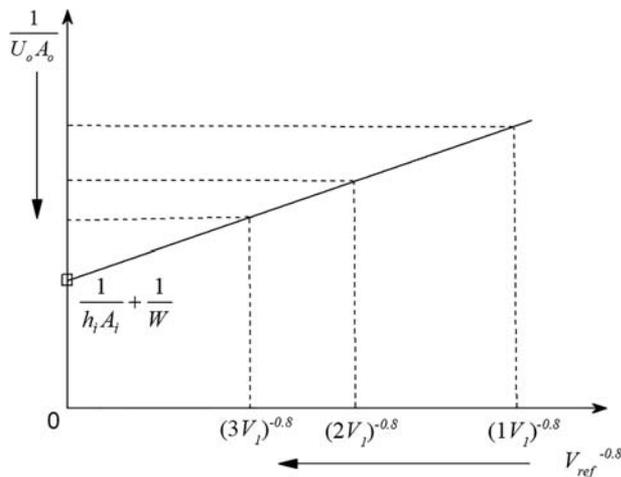|	R134A		R410A				
	Evaporation	Condensation	Evaporation			Condensation	
Temperature (°C)	6	45	6	10	35	40	45
Pressure (kPa)	361.98	1159.9	965.29	1088.4	2144.9	2425.6	2733.5
Liquid density ρ_l (kg/m^3)	1274.7	1125.1	1145.4	1128.4	1005.1	975.33	942.88
Vapor density ρ_v (kg/m^3)	17.717	57.657	36.347	41.177	87.455	101.71	118.66
Liquid thermal conductivity k_l (W/m K)	0.089367	0.072575	0.099645	0.097373	0.083585	0.080914	0.078276
Liquid viscosity μ_l (Pa s)	2.4697×10^{-4}	1.5139×10^{-4}	1.5000×10^{-4}	1.4276×10^{-4}	1.0303×10^{-4}	9.5861×10^{-5}	8.8817×10^{-5}
Latent heat of vaporization h_{lv} (kJ/kg)	199.95	157.58	218.63	213.24	172.67	162.55	151.39
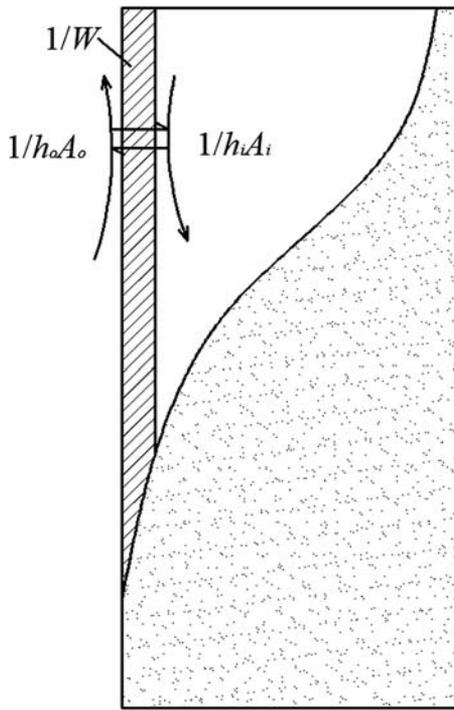
Fig. 3 Thermal resistance model for a circular tube

Fig. 4 Theoretical basis of the Wilson plot method

Fig. 5 Wilson plot results of two stainless steel enhanced tubes
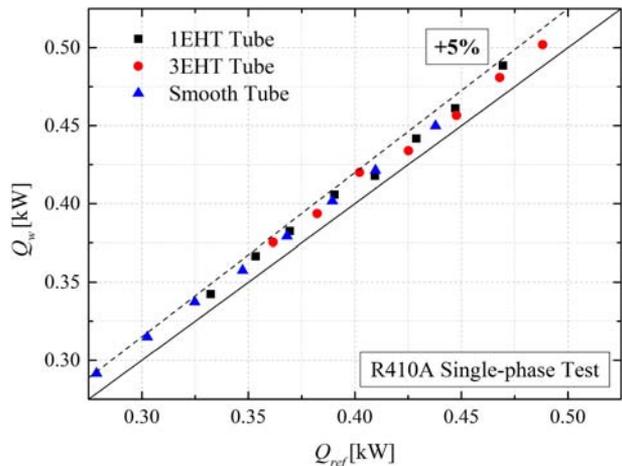
Fig. 6 Single-phase heat balance measurement

During the Wilson plot method evaluation, the refrigerant mass flux is constant at 200 kg/(m²s), and the water mass flux ranges from 600 to 900 kg/(m²s) (corresponding to Reynolds number from 3200 to 4800). According to the experimental results shown in Fig. 5, the enhancement ratio of the 1EHT tube is 2.03 and 3EHT tube enhancement ratio is 1.81.

In this study, the heat balance of the test section was evaluated using single-phase experiments in order to ensure the accuracy of the two-phase experimental results. As is shown in Fig. 6, the heat loss is well controlled within 5% (comparing the heat flux of the refrigerant and water). The uncertainties of measurements and calculated parameters are listed in Table 3. A detailed description of the experimental uncertainties is given in Ref. [24].

Results and Discussion

Single-Phase Heat Transfer. Figure 7(a) shows the single-phase variation of Nusselt number with Reynolds number in a
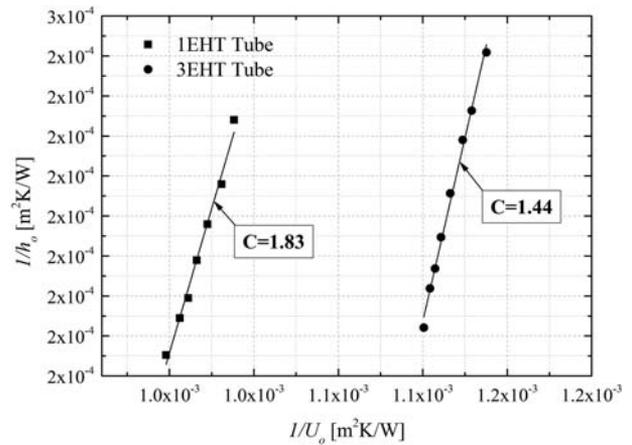
Table 3 The accuracy for primary measurements and dependent values

Primary measurements	
Diameter	±0.02 mm
Length	±0.5 mm
Temperature	±0.1 K
Pressure, range: 0–5000 kPa	±0.075% of full scale
Differential pressure: 0–50 kPa	±0.075% of full scale
Water flow rate, range: 0–1000 kg/h	±0.2% of reading
Refrigerant flow rate, range: 0–130 kg/h	±0.2% of reading
Dependent values	
Mass flux G_{ref}, kg/(m²s)	±1.04%
Heat flux q, kW/m²	±2.39%
Vapor quality x	±4.38%
Heat transfer coefficient h, W/(m²s)	±6.34%

stainless steel smooth tube and 1EHT tube; each with a 12.7-mm-OD, using R134A and R410A. The Nu number of the 1EHT tube is much higher at the same Re number. The enhancement of single-phase heat transfer coefficient is caused by swirling flow in the dimples and petal array. In addition, strong swirling enhances interfacial turbulence and disrupts the boundary layer. It can be seen that the single-phase heat transfer coefficients of the tested tubes have little difference using R134A and R410A. Figure 7(b) compares the experimental Nu numbers with the
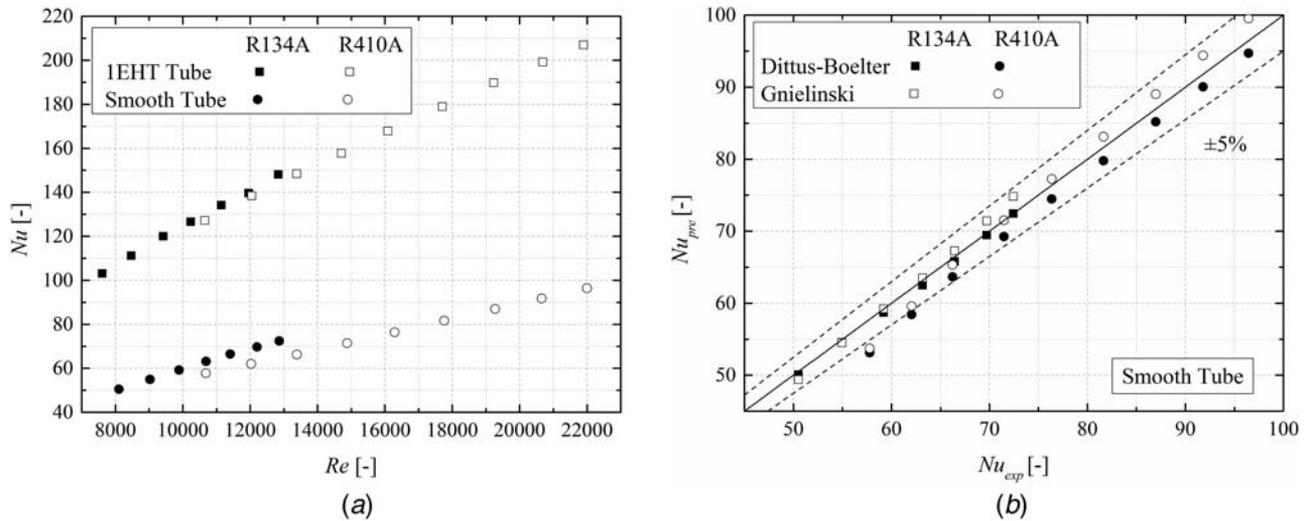
Fig. 7 The single-phase Nu number in a stainless steel smooth tube and 1EHT tube for 12.7-mm-OD

empirical correlations of Dittus–Boelter [29] and Gnielinski [27] for smooth tube; the results fit well with the predicted values with an error band ±5%.

Condensation Heat Transfer. Condensation heat transfer characteristics were evaluated inside 1EHT, 3EHT, and a smooth tube using R134A and R410A. Figure 8 shows the variation of the average heat transfer coefficients as a function of mass flux for a saturation temperature of 45 °C. It is observed that the two enhanced tubes produce better heat transfer performances over the tested range of mass flux; this is the result of its larger heat transfer surface area. It appears that some of the condensate liquid film on the bottom surface of the enhanced tubes was disrupted by the dimples/rectangle cavities and this increases the turbulence. The heat transfer coefficients increase slightly with the increase of mass flux. It appears that for low mass flux, the flow pattern is stratified flow; the effect of the mass flux on the condensation heat transfer coefficient is weak and negligible. It can be seen that the condensation heat transfer coefficient increases gradually for mass flux values over 120 kg/m²s. This can be explained by the liquid film thickness decreasing with the mass flux increasing; this results in a decrease of liquid thermal resistance. Moreover, the

vapor velocity increases and results in an increase in the shear stress on the liquid–vapor interface; this leads to more droplet entrainment. Enhancement of the condensation heat transfer coefficient results from the decrease of the liquid thermal resistance and the increase of the two-phase flow velocity.

Condensation heat transfer coefficient of the 1EHT tube is approximately 1.64–1.95 times than that of the smooth tube and for the 3EHT tube it is approximately 1.42–1.57 times. Reasons for the enhanced heat transfer in the 1EHT tube include increased heat transfer surface area of enhanced tubes, decreasing heat transfer resistance (dimples of the 1EHT tube can destroy the liquid film of the boundary layer), the structure of the 1EHT tube promotes condensate drainage from the boundary to the center by the shear stress, and enhanced mixing and turbulence. Finally, a thinner liquid film is formed on the surface of the enhanced tubes which causes an increase to the heat transfer coefficient. However, the rectangular cavities of 3EHT are an inefficient method to the enhancement of the condensation heat transfer coefficient since the condensate liquid remains on the bottom of the rectangular cavities, so the flow turbulence is weakened.

Finally, the condensation heat transfer coefficient of the smooth tube was compared with three existing correlations (Shah correlation [30], Cavallini et al. correlation [22], and Dorao and
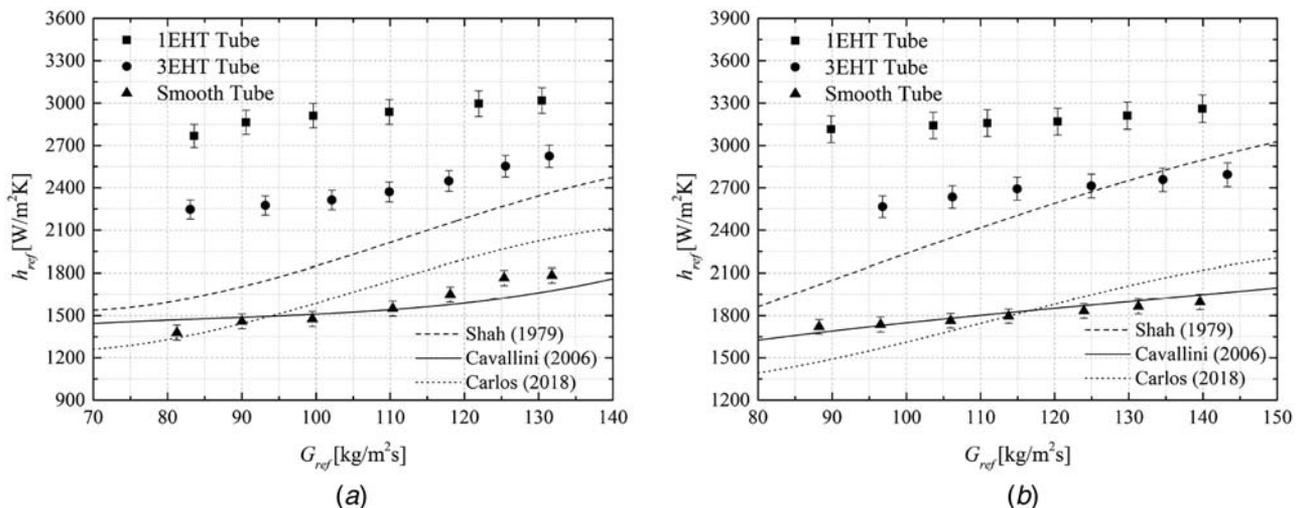

Fig. 8 Condensation heat transfer coefficient as a function of mass flux in two enhanced tubes and a smooth tube using (a) R134A condensation test and (b) R410A condensation test

Table 4 Predictive accuracy of the heat transfer correlations (_MAD_[a])

Condensation _MAD_	Dittus and Boelter [29] 23.7%	Shah [30] 8.5%	Dorao and Fernandino [31] 15.1%
Evaporation _MAD_	Liu and Winterton [33] 3.06%	Kandlikar [34] 13.89%	Wojtan et al. [23] 10.90%

[a] $MAD = \frac{1}{n} \sum_{1}^{n} \frac{|h_{exp} - h_{pre}|}{h_{exp}} \times 100\%$

Fernandino correlation [31]) in Fig. 8. It is noticed that the Cavallini et al. correlation [22] shows better predictive ability (at a low mass flux) than the other two condensation heat transfer correlations (regardless if R134A or R410A is used). Table 4 shows the mean absolute deviations (_MAD_) between the predictive values and experimental values. Cavallini et al. correlation [22] produces a mean absolute deviation of 8.5%, while a larger scatter is determined when using the Shah correlation [30] or the Dorao and Fernandino correlation [31]. This is probably due to the fact that they tend to be used in forced convective condensation and it is not accurate at a low mass flux. It is concluded that the condensation heat transfer coefficient of two enhanced tubes cannot be correlated with the empirical correlations.

Evaporation Heat Transfer. Figure 9 presents the evaporation heat transfer coefficient as a function of mass flux for 1EHT, 3EHT, and smooth stainless steel tubes when using R134A and R410A. Among all three test tubes, the heat transfer coefficient of the 1EHT tube is the largest, followed by the 3EHT tube and finally the smooth tube. The evaporation heat transfer coefficient of the enhanced tubes is in the range of 1.04–1.42 times than that of the smooth tube. The heat transfer enhancement is caused by the larger heat transfer area of enhanced tubes; additionally, the dimples and petal arrays in the surface of enhanced tubes generate more nucleation sites and swirl turbulence, which also increases the heat transfer coefficient. The surface structure also creates stronger interfacial turbulence and boundary layer disruption. Unlike the condensation results, the evaporation heat transfer coefficient increases significantly with increasing mass flux. On one hand, the low vapor density at a low saturation temperature tends to increase vapor velocity and this enhances the flow boiling heat transfer. On the other hand, a larger mass flux requires more heat flux, which in turn requires a greater degree of superheat; the

greater degree of superheat has a large effect on nucleate boiling. As far as the experimental conditions discussed in this paper are concerned, the increase of the heat flux and the degree of superheat has a strengthening effect on nucleate boiling. It is speculated (based on the Wojtan et al. [32] flow pattern map) that the 1EHT enhanced tube could achieve a transformation from stratified flow to stratified-wavy flow earlier due to the dimple enhancement units. The same is not true for the 3EHT tube; it doesnot show enhanced evaporation heat transfer for low mass flux values. As is shown in Fig. 9, the evaporation heat transfer coefficients of the 3EHT tube is only slightly larger than that of a smooth tube even though there is a larger heat transfer area ratio (1.25). The rectangular cavities on the surface of the 3EHT tube are obviously more inefficient for these evaporation conditions. This may be explained by the depth of the ribs; the rib height is less than liquid film thickness and the shorter ribs couldnot change the flow direction and cause strong swirls.

Evaporation is composed of nucleate or convective components or both, at low mass flux the nucleate flow regime is dominant. Comparison of the evaporation heat transfer coefficients' predictive effect is presented in Fig. 9; Liu and Winterton correlation [33], Kandlikar correlation [34], and Wojtan et al. correlation [23] show good predictive ability for evaporation heat transfer at a low mass flux. The predictive accuracy of evaporation heat transfer correlations is given in Table 4. The accuracy of the Kandlikar correlation [34] decreases with increasing the mass flux, while the Liu and Winterton correlation [33] can predict all experiment data points with a relatively small deviation.
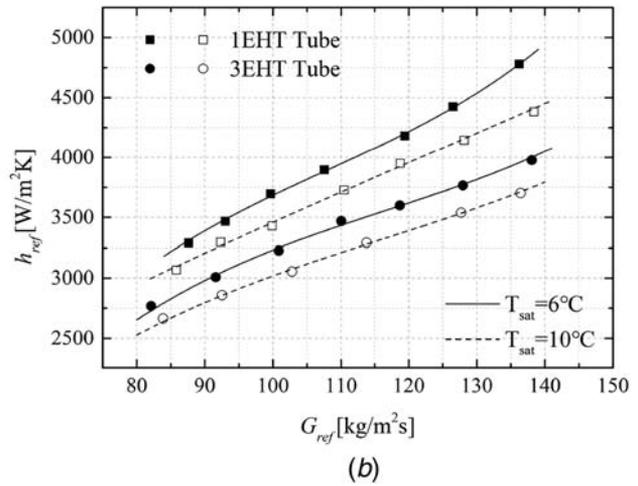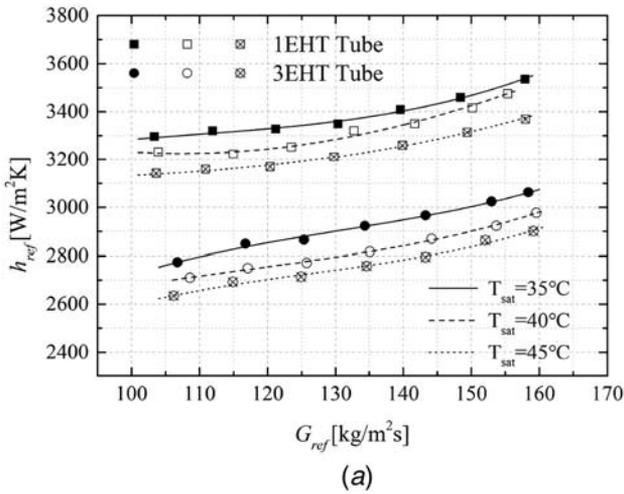
For evaporation heat transfer in the tubes that were evaluated, R410A performs much better than R134A. This is because of the larger shear stress that is present in R410A between the liquid phase and vapor phase; this produces a thinner liquid film than that which is produced using R134A. In addition, the higher liquid thermal conductivity and higher vapor density also contribute to the higher heat transfer coefficients.

Effect of Saturation Temperature and Tube Diameter on Heat Transfer Coefficients. Figure 10 displays the effect of saturation temperature on the condensation and evaporation heat transfer coefficient. The condensation heat transfer coefficient decreases as the saturation temperature rises for both the 1EHT and 3EHT tubes. This is due to the liquid thermal conductivity being lower at higher saturation temperatures, which results in higher liquid thermal resistance. In addition, the higher saturation temperature leads to a higher vapor density, which creates shear stress between the liquid film and tube wall; this weakens the
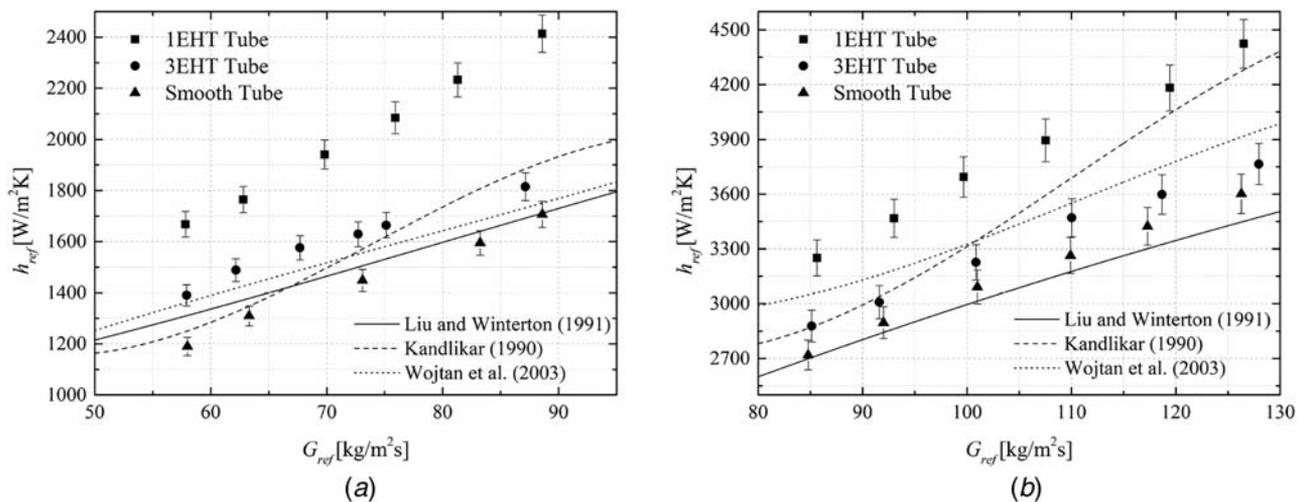
Fig. 9 Evaporation heat transfer coefficient as a function of mass flux in two enhanced tubes and a smooth tube using (_a_) R134A evaporation test and (_b_) R410A evaporation test

Fig. 10 The effect of saturation temperature on heat transfer coefficients in the 1EHT tube and 3EHT tube: (a) condensation and (b) evaporation

interaction of the liquid–vapor interface. The low latent heat of vaporization present under a high saturation temperature is also a significant factor affecting the heat transfer characteristics. As shown in Fig. 10, the condensation heat transfer coefficients for $T_{sat} = 35\,^{\circ}\text{C}$ and the evaporation heat transfer coefficients for $T_{sat} = 6\,^{\circ}\text{C}$ are higher under the test conditions.

From Fig. 11, it can be seen that for the most part, the heat transfer coefficients of the 12.7-mm-OD tubes are higher than that of 15.88-mm-OD tubes. The solid lines denote the measured heat transfer coefficients in R410A for 1EHT and smooth tube of 12.7-mm-OD; the dotted line symbol denotes those of tubes of 15.88-mm-OD. This can partially be explained by the fact that as tube diameters increased, the condensation and evaporation heat transfer characteristics are more dominated by gravity. At a low mass flux, the flow regime is mainly stratified or stratified-wavy; the gravitational force is more dominant than viscosity and shear forces; and the liquid film deposits more at the bottom of the tube, which serves as a thermal resistance and decreases the heat transfer coefficient. Furthermore, the effect of the surface tension and shear stress forces both the gas–liquid interface and the liquid film/tube wall to be reduced for two-phase flow at a low mass flux. An interesting phenomenon shown in Fig. 11 is that the heat transfer coefficient of the 12.7-mm-OD smooth tube is less than that of the 15.88-mm-OD 1EHT tube under the same test

conditions. This is because the dimples and protrusions have obvious and significant enhancement effect for condensation and evaporation heat transfer characteristics under a low mass flux. It can be concluded that the heat transfer coefficient decreases with increasing the tube diameter.

An enhancement factor (EF) is defined as a ratio of the heat transfer coefficient for an enhanced tube and smooth tube (having same outer tube diameter) with similar test conditions

$$EF = \frac{h_e}{h_s} \qquad (11)$$

As is shown in Fig. 12(a), the enhancement factor for condensation of the 1EHT tube varies from 1.7 to 2.0 for 15.88-mm-OD and 12.7-mm-OD tube using R134A and R410A, while those for 3EHT tube it varied from 1.4 to 1.6 as the mass flux increases from 80 to 140 kg/(m²s). The EF decreases gradually with an increase of mass flux, indicating a good enhancement effect at low mass flux. For evaporation, unlike condensation, there is a larger enhancement factor using R134A as the working fluid. Figure 12(b) shows that the EF of the 1EHT tube (with R134A and R410A) is approximately 1.4 and 1.2, respectively. In summary, the 1EHT and 3EHT tubes present excellent condensation heat transfer performance at relatively low mass flux values.
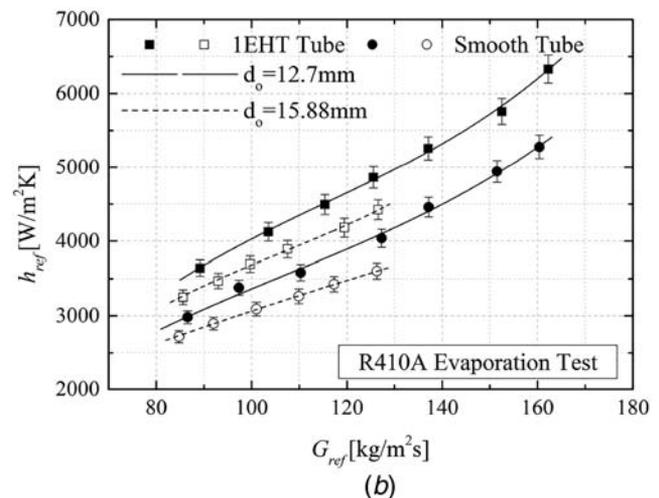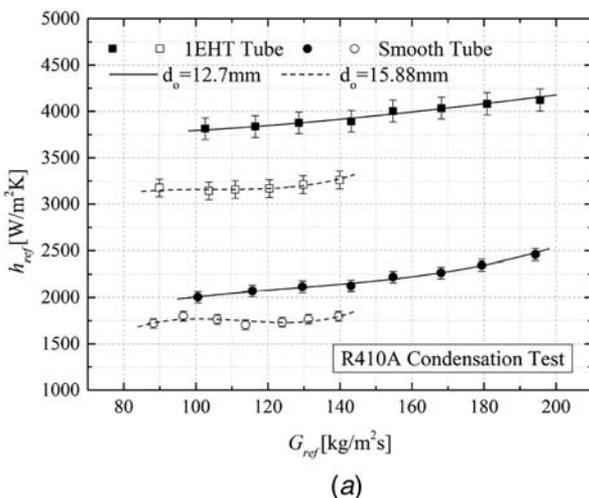
Fig. 11 The effect of tube diameter on heat transfer coefficients in the 1EHT tube and smooth tube: (a) condensation and (b) evaporation
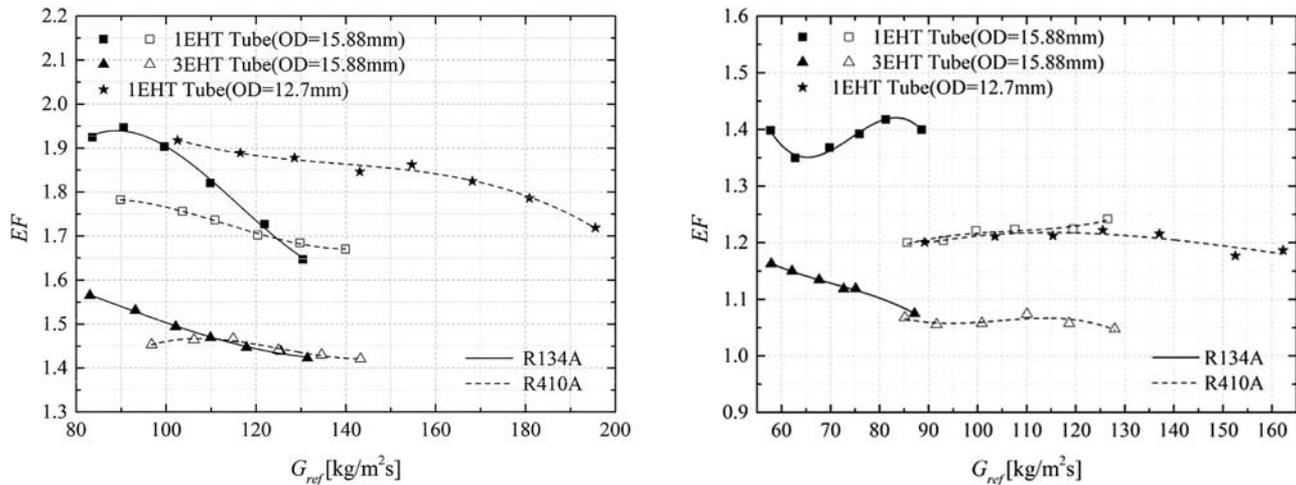
Fig. 12 Heat transfer enhancement factor as a function of mass flux in R134A and R410A for the enhanced tubes: (a) condensation and (b) evaporation

Conclusions

An experimental investigation of condensation ($T_{sat} = 45\,^{\circ}\text{C}$) and evaporation ($T_{sat} = 6\,^{\circ}\text{C}$) heat transfer characteristics was performed in a smooth tube and two three-dimensional enhanced tubes (1EHT, 3EHT) using R134A and R410A. The following conclusions are made

(1) For condensation, the 1EHT and 3EHT tube produces higher heat transfer coefficients than a stainless steel smooth tube. Cavallini et al. correlation [22] shows a good predictive ability for a smooth tube.

(2) For evaporation, the heat transfer coefficients increase significantly with increasing mass flux. It can be speculated that the higher vapor velocities will lead to strong interfacial turbulence and that the surface structure increases the nucleation sites. Liu and Winterton correlation [33] can accurately predict the current evaporation experiment data with a mean absolute deviation of 3.06%.

(3) R410A presents better heat transfer characteristics than R134A due to its higher vapor density and liquid thermal conductivity. The low saturation temperature and small tube diameter also have a beneficial effect on the heat transfer characteristics.

(4) The condensation heat transfer coefficient for 1EHT and 3EHT tubes are 70–200% and 40–60% higher than the smooth tube, while for evaporation they are 20–45% and 5–20% higher at similar test conditions.

Funding Data

Nomenclature

f = Fanning friction factor, —
h = heat transfer coefficient, W/(m^2 K)
k = thermal conductivity, W/(m K)
l = heat length, m
m = mass flow rate, kg/s
q = heat flux, W/m^2
x = vapor quality, —
A = heat transfer area, —
C = enhancement ratio, —
D = inner diameter of the outer tube, m
H = enthalpy, kJ/kg
Q = heat transfer amount, W
T = temperature, K

U = total heat transfer coefficient, W/(m^2 K)
c_p = specific heat, J/(kg K)
d_h = hydraulic diameter, m
h_{lv} = latent heat of vaporization, J/kg
A_i = inner surface area of the test tube, m^2
A_o = outer surface area of the test tube, m^2
d_i/ID = inner diameter of the test tube, m
d_o/OD = outer diameter of the test tube, m
EF = enhancement factor, —
EHT = enhanced heat transfer tube, —
G/V = mass flux, kg/(m^{2}s)
$LMTD$ = logarithmic mean temperature, K
MAD = mean absolute deviation, —
Pr = Prandtl number, —
Re = Reynolds number, —

Greek Symbols

γ = heat loss, —
μ = dynamic viscosity, Pa s
ρ = density, kg/m^3

Subscripts

e = enhanced
exp = experiment
i = inner
in = inlet
l = liquid phase
o = outer
out = outlet
pre = preheat section
ref = refrigerant
s = smooth
sat = saturated
v = vapor phase
w = water

References

[1] Wu, Z., Sunden, B., Wang, L., and Li, W., 2014, "Convective Condensation Inside Horizontal Smooth and Microfin Tubes," ASME J. Heat Transfer, **136**(5), p. 051504.

[2] Li, W., Tang, W., Chen, J., Zhu, H., Kukulka, D. J., He, Y., Sun, Z., Du, J., and Zhang, B., 2018, "Convective Condensation in Three Enhanced Tubes With Different Surface Modifications," Exp. Therm. Fluid Sci., **97**, pp. 79–88.

[3] Li, W., Ma, X., Sun, Z.-c., He, Y., Sherif, S. A., Zhang, J.-h., and Zhu, H.-t., 2019, "Evaporation Heat Transfer Characteristics of R410A Inside Horizontal Three-Dimensional Enhanced Tubes," Int. J. Therm. Sci., **137**, pp. 456–466.

[4] Chen, J., and Li, W., 2018, "Local Flow Boiling Heat Transfer Characteristics in Three-Dimensional Enhanced Tubes," Int. J. Heat Mass Transfer, 121, pp. 1021–1032.

[5] Sun, Z.-c., Li, W., Guo, R.-h., He, Y., and Kukulka, D. J., 2018, "Condensation Heat Transfer in Horizontal Three Dimension Two-Layer Two Side Enhanced Tubes," Int. J. Heat Mass Transfer, 127, pp. 141–145.

[6] Kondou, C., Mishima, F., and Koyama, S., 2015, "Condensation and Evaporation of R32/R1234ze(E) and R744/R32/R1234ze(E) Flow in Horizontal Microfin Tubes," Hvac & R Res., 21(5), pp. 564–577.

[7] Ewim, D. R. E., Meyer, J. P., and Noori Rahim Abadi, S. M. A., 2018, "Condensation Heat Transfer Coefficients in an Inclined Smooth Tube at Low Mass Fluxes," Int. J. Heat Mass Transfer, 123, pp. 455–467.

[8] Singh, S., and Kukreja, R., 2018, "Experimental Heat Transfer Coefficient and Pressure Drop During Condensation of R-134a and R-410A in Horizontal Micro-Fin Tubes," Int. J. Air-Cond. Refrig., 26(3), p. 1850022.

[9] Goto, M., Inoue, N., and Ishiwatari, N., 2001, "Condensation and Evaporation Heat Transfer of R410A Inside Internally Grooved Horizontal Tubes," Int. J. Refrig., 24(7), pp. 628–638.

[10] Kim, Y., Seo, K., and Jin, T. C., 2002, "Evaporation Heat Transfer Characteristics of R-410A in 7 and 9.52 mm Smooth/Micro-Fin Tubes," Int. J. Refrig., 25(6), pp. 716–730.

[11] Miyara, A., Otsubo, Y., and Ohtsuka, S., 2002, "Evaporation Heat Transfer of R410A in Herringbone Micro Fin Tubes, Thermophysical Properties and Transfer Processes of New Refrigerants," CDROM, France, pp. 314–319.

[12] Kim, N. H., 2016, "Condensation Heat Transfer and Pressure Drop of R-410A in a 7.0 mm O.D. Microfin Tube at Low Mass Fluxes," Heat Mass Transfer, 52(12), pp. 2833–2847.

[13] Sarmadian, A., Shafaee, M., Mashouf, H., and Mohseni, S.G., 2017, "Condensation Heat Transfer and Pressure Drop Characteristics of R-600a in Horizontal Smooth and Helically Dimpled Tubes," Exp. Therm. Fluid Sci., 86, pp. 54–62.

[14] Aroonrat, K., and Wongwises, S., 2017, "Experimental Study on Two-Phase Condensation Heat Transfer and Pressure Drop of R-134a Flowing in a Dimpled Tube," Int. J. Heat Mass Transfer, 106, pp. 437–448.

[15] Aroonrat, K., and Wongwises, S., 2018, "Condensation Heat Transfer and Pressure Drop Characteristics of R-134a Flowing Through Dimpled Tubes With Different Helical and Dimpled Pitches," Int. J. Heat Mass Transfer, 121, pp. 620–631.

[16] Aroonrat, K., and Wongwises, S., 2019, "Experimental Investigation of Condensation Heat Transfer and Pressure Drop of R-134a Flowing Inside Dimpled Tubes With Different Dimpled Depths," Int. J. Heat Mass Transfer, 128, pp. 783–793.

[17] Li, W., Sun, Z.-c., Guo, R.-h., Ma, X., Liu, Z.C., Kukulka, D.J., Ayub, Z., Chen, W., and He, Y., 2019, "Condensation Heat Transfer of R410A on Outside of Horizontal Smooth and Three-Dimensional Enhanced Tubes," Int. J. Refrig., 98, pp. 1–14.

[18] Dalkilic A, S., Celen, A., Cebi, A., and Wongwises, S., 2016, "Empirical Correlations for the Determination of R134a's Convective Heat Transfer Coefficient in Horizontal and Vertical Evaporators Having Smooth and Corrugated Tubes," Int. Commun. Heat Mass Transfer, 76, pp. 85–97.

[19] Lu, Q., Chen, D., Li, C., and He, X., 2017, "Experimental Investigation on Flow Boiling Heat Transfer in Conventional and Mini Vertical Channels," Int. J. Heat Mass Transfer, 107, pp. 225–243.

[20] Jingzhi, Z., Naixiang, Z., Wei, L., and Yang, L., 2018, "An Experimental Study of R410A Condensation Heat Transfer and Pressure Drops Characteristics in Microfin and Smooth Tubes With 5 mm OD," Int. J. Heat Mass Transfer, 125, pp. 1284–1295.

[21] Guo, S. P., Wu, Z., Li, W., Kukulka, D., Sundén, B., Zhou, X.P., Wei, J.J., and Simon, T., 2015, "Condensation and Evaporation Heat Transfer Characteristics in Horizontal Smooth, Herringbone and Enhanced Surface EHT Tubes," Int. J. Heat Mass Transfer, 85, pp. 281–291.

[22] Cavallini, A., Del C, D., Doretti, L., Matkovic, M., Rossetto, L., Zilio, C., and Censi, G., 2006, "Condensation in Horizontal Smooth Tubes: A New Heat Transfer Model for Heat Exchanger Design," Heat Transfer Eng., 27(8), pp. 31–38.

[23] Wojtan, L., Ursenbacher, T., and Thome, J. R., 2005, "Investigation of Flow Boiling in Horizontal Tubes: Part II—Development of a New Heat Transfer Model for Stratified-Wavy, Dryout and Mist Flow Regimes," Int. J. Heat Mass Transfer, 48(14), pp. 2970–2985.

[24] Li, W., Chen, J. X., Zhu, H., Kukulka, D. J., and Minkowycz, W. J., 2017, "Experimental Study on Condensation and Evaporation Flow Inside Horizontal Three Dimensional Enhanced Tubes," Int. Commun. Heat Mass Transfer, 80, pp. 30–40.

[25] Wang, X., Ho, J. Y., Leong, K. C., and Wong, T. N., 2018, "Condensation Heat Transfer and Pressure Drop Characteristics of R-134a in Horizontal Smooth Tubes and Enhanced Tubes Fabricated by Selective Laser Melting," Int. J. Heat Mass Transfer, 126, pp. 949–962.

[26] Lemmon, E. W., Huber, M. L., and Mclinden, M. O., 2010, NIST Standard Reference Database 23: Reference Fluid Thermodynamic and Transport Properties-REFPROP. 9.0. NIST NSRDS.

[27] Gnielinski, V., 1976, "New Equations for Heat and Mass Transfer in Turbulent Pipe and Channel Flow," Int. Chem. Eng., 16(2), pp. 8–16.

[28] Petukhov, B. S., 1970, "Heat Transfer and Friction in Turbulent Pipe Flow With Variable Physical Properties," Adv. Heat Transfer, 6, pp. 503–564.

[29] Dittus, F. W., and Boelter, L. M. K., 1985, "Heat Transfer in Automobile Radiator of the Tubular Type," Int. Commun. Heat Mass Transfer, 12(1), pp. 3–22.

[30] Shah, M. M., 1979, "A General Correlation for Heat Transfer During Film Condensation Inside Pipes," Int. J. Heat Mass Transfer, 22(4), pp. 547–556.

[31] Dorao, C. A., and Fernandino, M., 2018, "Simple and General Correlation for Heat Transfer During Flow Condensation Inside Plain Pipes," Int. J. Heat Mass Transfer, 122, pp. 290–305.

[32] Wojtan, L., Ursenbacher, T., and Thome, J. R., 2005, "Investigation of Flow Boiling in Horizontal Tubes: Part I—A New Diabetic Two-Phase Flow Pattern Map," Int. J. Heat Mass Transfer, 48(14), pp. 2955–2969.

[33] Liu, Z., and Winterton, R. H. S., 1991, "A General Correlation for Saturated and Subcooled Flow Boiling in Tubes and Annuli, Based on a Nucleate Pool Boiling Equation," Int. J. Heat Mass Transfer, 34(11), pp. 2759–2766.

[34] Kandlikar, S. G., 1990, "A General Correlation for Saturated Two-Phase Flow Boiling Heat Transfer Inside Horizontal and Vertical Tubes," ASME J. Heat Transfer, 112(1), pp. 219–228.